PHYSICAL REVIEW E **91**, 042918 (2015)

Analytical stability boundaries of an injected two-polarization semiconductor laser

Gaetan Friart,[1,*] Athanasios Gavrielides,[2] and Thomas Erneux[1]

[1]*Université Libre de Bruxelles, Optique Nonlinéaire Théorique, Campus Plaine, C.P. 231, 1050 Bruxelles, Belgium*

[2]*University of New Mexico, Center for High Technology Materials, Albuquerque, New Mexico 87131-0001, USA*

(Received 15 December 2014; published 30 April 2015)

The classical problem of a semiconductor laser subject to polarized injection is revisited. From the laser rate equations for the transverse electric (TE) and transverse magnetic (TM) modes, we first determine the steady states. We then investigate their linear stability properties and derive analytical expressions for the steady, saddle-node, and Hopf bifurcation points. We highlight conditions for bistability between pure- and mixed-mode steady states for the laser subject to either TE or TM injection. To our knowledge, the first case has not been documented yet. An important parameter is the ratio of the polarization gain coefficients and we explore its effect on the stability and bifurcation diagrams.

DOI: 10.1103/PhysRevE.91.042918 PACS number(s): 05.45.−a, 42.55.Px, 42.60.Lh, 42.65.Sf

I. INTRODUCTION

In semiconductor lasers (SLs), there are two allowed polarization modes constrained by the waveguide geometry of the laser cavity. They are referred to as the transverse electric (TE) mode, with the electric field parallel to the junction plane, and the transverse magnetic (TM) mode, with the magnetic field parallel to the junction plane. Under normal stress-free conditions the laser output is TE polarized because the mode has a larger mode-confinement factor in the waveguide and a higher reflectivity at the facets. However, the TM mode can be promoted to compete with the TE mode by introducing a small amount of lattice deformation into the active layer that changes the band structure and thereby enhances the optical gain of the TM mode relative to that of the TE mode [1–3]. In the mid-1980s [4,5], polarization bistability was successfully achieved showing large hysteresis loops between the two orthogonal directions as the pump current was varied. Within the hysteresis loop, the polarization of the laser output could be switched by current pulse injection. Soon, switching between TE and TM polarization states in the output of a semiconductor laser was experimentally obtained through injection locking from external TM-polarized radiation [6]. The polarization bistability phenomenon was further studied by Mori *et al.* [7–9].

At the same time, injection locking induced by a TE external signal appeared as an interesting method to reduce laser linewidth [10], enhance the modulation bandwidth [11], synchronize lasers for microwave generation [12,13], or measure the linewidth enhancement factor [14,15]. The injection locking phenomenon in Fabry-Perot cavity SLs has been the topic of a large number of papers [16]. Theoretical and experimental studies have revealed several forms of pulsating intensity oscillations [17]. A notable feature of the optically injected laser is that its response can be described by three nonlinear ordinary differential equations. This then motivated quantitative comparisons between experimental and numerical stability diagrams [18,19] that led to the observation of new dynamical regimes and the development of new engineering applications.

The relative simplicity of the laser rate equations compared to other laser dynamical problems has encouraged analytical approaches. Their main advantages are the possibility to clearly identify the effects of key parameters such as the linewidth enhancement factor or the pump [19]. They also provide insight on posing questions properly that numerical computations could have missed. To date, an analytical study of the injection laser problem with the two polarization modes is lacking. Our objective is to investigate both the case of the classical TE injection as well as the case of the TM injection. We find that pure- and mixed-mode steady states coexist in parameter space and exhibit both saddle-node and Hopf bifurcation instabilities.

Our work has been prompted by a recent study of the bistability properties of an optically injected two-mode laser (called a two-color laser [20]). The objective of the authors was to find out how such a laser can be used as an all-optical memory element for which fast switching between states is possible. They demonstrate experimentally that in the two-color laser a bistability between the injection locked (single-mode) state and a two-color equilibrium state (steady state) is possible. Remarkably, the mathematical formulation of the injected two-color laser is similar to the single longitudinal mode laser problem with its two polarizations. We also noted that two-mode models have successfully explained the switching between single-mode states with different polarizations in vertical-cavity surface-emitting lasers [21]. However, the evolution equations are more complex to analyze compared to the injected single-mode laser.

Furthermore, the injected semiconductor ring laser shows a number of similarities with our two polarization injection problem [22–24]. Indeed, the formulation of the problem is identical to the problem we are considering if the coupling of the clockwise and the counterclockwise modes due to scattering is ignored.

Two important parameters measure the differences between the total gains of the TE and TM modes. They are defined as

$$k \equiv \frac{G_2}{G_1} \leqslant 1 \quad \text{and} \quad \beta \equiv \frac{1}{2}\left(\frac{\gamma_2 G_1}{\gamma_1 G_2} - 1\right) \geqslant 0, \qquad (1)$$

where k is the ratio of the gain coefficients of the TM (G_2) and TE (G_1) modes. β measures the losses of the TM mode compared to the TE mode. It depends on both the ratio of the gains coefficients and the ratio of the cavity losses for

*gfriart@ulb.ac.be

the TM (γ_2) and TE (γ_1) modes. For both the TE and TM injection problems, we plan to, first, investigate the ideal case where $k = 1$ and $\beta = 0$ because it highlights some important conditions. It is also the case considered in Ref. [20] for the two-color laser. We then analyze the modification of the stability diagrams when $k < 1$ and $\beta > 0$. For mathematical simplicity, we assume $\gamma_1 = \gamma_2$ and concentrate on the effects of

$$k \equiv \frac{G_2}{G_1} \leqslant 1 \quad \text{and} \quad \beta \equiv \frac{1-k}{2k} \geqslant 0. \tag{2}$$

The plan of the paper is as follows. Sections II and III consider the cases of a single TE injection and a single TM injection, respectively. We determine the steady states and analyze their linear stability properties. Our results are summarized through stability diagrams in terms of the injection amplitude and the frequency detuning. Bifurcation diagrams showing the steady-state intensity as a function of the injection amplitude illustrate different forms of bistability.

II. TE INJECTION

The usual rate equations describing a semiconductor laser subject to TE-polarized optical injection consist of two equations, namely an equation for the complex TE electric field coupled to an equation for the carrier density. Here we take into account the two polarization modes of the laser and include a third equation for the complex TM electric field. This two-mode model has successfully been used in the case of a delayed optical feedback [25–29] and we recently showed that different models proposed in the literature reduce to the same dimensionless equations [30]. In the case of TE optical injection, the dimensionless rate equations are given by

$$\frac{dE_1}{dt} = (1 + i\alpha)NE_1 + \gamma \exp(i\Delta t), \tag{3}$$

$$\frac{dE_2}{dt} = k(1 + i\alpha)(N - \beta)E_2, \tag{4}$$

$$T\frac{dN}{dt} = P - N - (1 + 2N)(|E_1|^2 + |E_2|^2), \tag{5}$$

where E_1, E_2, and N are the amplitude of the TE electric field, the amplitude of the TM electric field, and carrier density, respectively. α is the linewidth enhancement factor, T is the ratio of carrier to cavity lifetimes, and P is the pump parameter above threshold; k and β are defined in Eq. (2). In addition, γ is the injection strength and Δ is the frequency detuning between the injected signal and the solitary laser. Introducing $E_1 = R_1 \exp(i\Delta t + i\phi_1)$ and $E_2 = R_2 \exp(i\phi_2)$ into Eqs. (3)–(5) leads to the following equations for R_1, ϕ_1, R_2, and N:

$$\frac{dR_1}{dt} = NR_1 + \gamma \cos(\phi_1), \tag{6}$$

$$\frac{d\phi_1}{dt} = -\Delta + \alpha N - \gamma R_1^{-1} \sin(\phi_1), \tag{7}$$

$$\frac{dR_2}{dt} = k(N - \beta)R_2, \tag{8}$$

$$T\frac{dN}{dt} = P - N - (1 + 2N)\left(R_1^2 + R_2^2\right). \tag{9}$$

The evolution of ϕ_2 passively depends on N and its equation is not shown.

We first compute the steady-state solutions of Eqs. (6)–(9). The pure-mode solution satisfies the conditions

$$\begin{aligned} (1):\ \ & R_2 = 0, \\ & \gamma = \sqrt{[N^2 + (-\Delta + \alpha N)^2]}R_1, \\ & R_1^2 = \frac{P - N}{1 + 2N} \geqslant 0. \end{aligned} \tag{10}$$

In order to analyze R_1^2 as a function of γ, we consider N as a parameter ($-1/2 < N \leqslant P$). Using (10), we first compute R_1^2 and then γ.

There exists a mixed-mode solution if $\beta < P$. It satisfies the conditions

$$\begin{aligned} (2):\ \ & N = \beta, \\ & R_2^2 = \frac{P - \beta}{1 + 2\beta} - R_1^2 \geqslant 0, \\ & \gamma = \sqrt{[\beta^2 + (-\Delta + \alpha\beta)^2]}R_1. \end{aligned} \tag{11}$$

We compute the two intensities as functions of γ by using R_1 as a parameter $[0 \leqslant R_1 \leqslant \sqrt{(P - \beta)/(1 + 2\beta)}]$. From (11), we first determine γ and then R_2.

A. Stability

1. TE steady state

From Eqs. (6)–(9), we formulate the linearized problem and determine the characteristic equation for the growth rate λ. One eigenvalue is

$$\lambda_1 = k(N - \beta) \tag{12}$$

and the remaining eigenvalues satisfy

$$\lambda^3 + a_1\lambda^2 + a_2\lambda + a_3 = 0, \tag{13}$$

where

$$\begin{aligned} a_1 &= -2N + \varepsilon\left(1 + 2R_1^2\right), \\ a_2 &= N^2 + (\Delta - N\alpha)^2 - 2\varepsilon\left(1 + 2R_1^2\right)N + 2R_1^2\varepsilon(1 + 2N), \\ a_3 &= \varepsilon\left\{\left(1 + 2R_1^2\right)(N^2 + (\Delta - N\alpha)^2) \right. \\ &\quad \left. + 2(1 + 2N)R_1^2[(\Delta - N\alpha)\alpha - N]\right\}, \end{aligned} \tag{14}$$

and $\varepsilon \equiv T^{-1}$. The Routh-Hurwitz conditions for the stability of the steady state are [31]

$$a_1 > 0, \quad a_3 > 0, \quad a_1a_2 - a_3 > 0. \tag{15}$$

We next assume that there exists a steady state that satisfies (15). A first change of stability may occur if $a_3 = 0$ [saddle-node (SN) bifurcation]. Equivalently,

$$\begin{aligned} &\frac{1 + 2P}{1 + 2N}X^2 + 2(P - N)\alpha X + \frac{1 + 2P}{1 + 2N}N^2 - 2N(P - N) \\ &\quad = 0, \end{aligned} \tag{16}$$

where $X \equiv \Delta - N\alpha$. Another change of stability is possible if $a_1a_2 - a_3 = 0$ [Hopf (H) bifurcation]. This condition is

$$0 = NX^2 + \varepsilon\alpha(P-N)X - \varepsilon\left(\frac{1+2P}{1+2N}\right)[2N^2 + \varepsilon(P-N)] + N^3 + \varepsilon(P-N)N + \varepsilon^2 N\left(\frac{1+2P}{1+2N}\right)^2. \quad (17)$$

Equations (16) and (17) were derived in Ref. [32] and they are independent of k and β. Condition (12) is new and requires $N < \beta$ for stability.

2. TE+TM steady state

From Eqs. (6)–(9), we formulate the linearized problem and determine the following characteristic equation for the growth rate λ:

$$\lambda^4 + a_1\lambda^3 + a_2\lambda^2 + a_3\lambda + a_4 = 0, \quad (18)$$

where

$$a_1 = -2\beta + \varepsilon\frac{1+2P}{1+2\beta},$$
$$a_2 = \left[2\varepsilon(1+2\beta)R_1^2 + \beta^2 + (\Delta-\alpha\beta)^2 - \varepsilon\frac{1+2P}{1+2\beta}2\beta + 2\varepsilon k R_2^2(1+2\beta)\right],$$
$$a_3 = \varepsilon\left\{2(1+2\beta)R_1^2[(\Delta-\alpha\beta)\alpha - \beta] + \frac{1+2P}{1+2\beta}[\beta^2 + (\Delta-\alpha\beta)^2] - 4kR_2^2(1+2\beta)\beta\right\},$$
$$a_4 = 2\varepsilon k R_2^2(1+2\beta)[\beta^2 + (\Delta-\alpha\beta)^2]. \quad (19)$$

The Routh-Hurwitz conditions for the stability of the steady state are [31]

$$a_1 > 0, \quad a_3 > 0, \quad a_4 > 0, \quad a_1a_2a_3 - a_3^2 - a_1^2a_4 > 0. \quad (20)$$

B. Case $\beta = 0$

Of particular interest is the case of equal gains for the two modes ($k = 1$ and $\beta = 0$) because it corresponds to the model used for the two-color laser (without gain saturation) and it simplifies the mixed-mode equations. The coefficients of the characteristic equations (19) reduce to

$$\begin{aligned} a_1 &= \varepsilon(1+2P),\\ a_2 &= 2\varepsilon P + \Delta^2,\\ a_3 &= \varepsilon\left[2R_1^2\Delta\alpha + (1+2P)\Delta^2\right],\\ a_4 &= 2\varepsilon R_2^2\Delta^2. \end{aligned} \quad (21)$$

The stability conditions are

$$(1): 2R_1^2\Delta\alpha + (1+2P)\Delta^2 > 0 \quad (22)$$

$$(2): \left\{(1+2P)(2\varepsilon P + \Delta^2)\left[2R_1^2\Delta\alpha + (1+2P)\Delta^2\right] - \left[2R_1^2\Delta\alpha + (1+2P)\Delta^2\right]^2 - (1+2P)^2 2\varepsilon R_2^2\Delta^2\right\} > 0. \quad (23)$$

The first condition is satisfied if

$$\Delta > 0 \text{ or}$$
$$\Delta < 0 \quad \text{and} \quad R_1^2 < -\frac{(1+2P)\Delta}{2\alpha}. \quad (24)$$

The second condition requires

$$R_1^2 < \frac{(1+2P)}{2\Delta\alpha^2}[\alpha 2\varepsilon P - \alpha\Delta^2 + (1+2P)\varepsilon\Delta] \quad (25)$$

and

$$\Delta[\alpha 2\varepsilon P - \alpha\Delta^2 + (1+2P)\varepsilon\Delta] > 0. \quad (26)$$

The two-mode solution bifurcates from the pure-mode solution at

$$\gamma = |\Delta|\sqrt{P} \quad (27)$$

and are the lines SB_2 in Fig. 1. A Hopf bifurcation from the two-mode solution is possible if (24) and (26) are satisfied. It

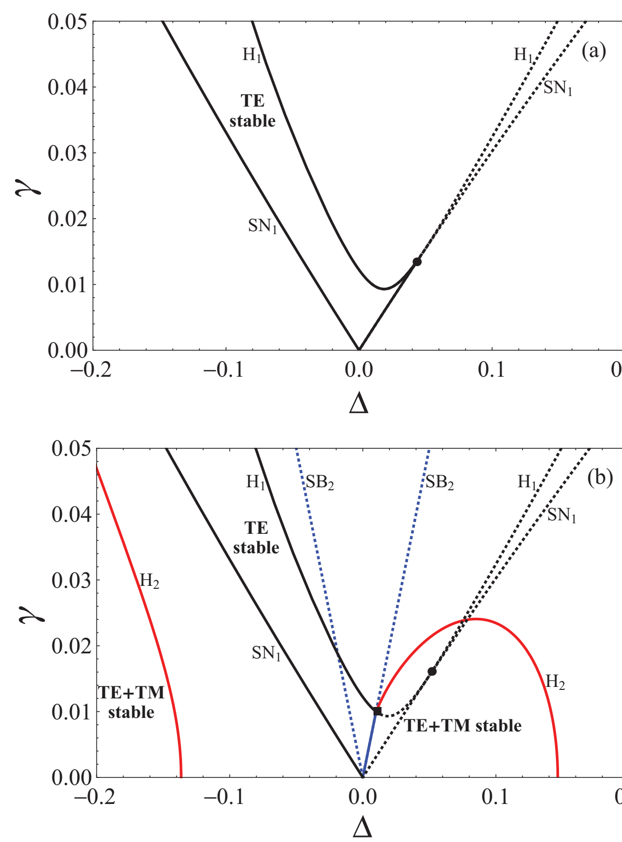

FIG. 1. (Color online) Stability diagram for $\beta = 0$. In (a), only the TE mode is considered for the slave laser and, in (b), both the TE and TM modes are considered for the slave laser. SN_1 is the saddle-node bifurcation point where the pure mode is locked. SB_2 is the steady-state bifurcation point from the pure-mode solution to the two-mode solution. H_1 and H_2 are Hopf bifurcations from the pure-mode and two-mode steady state, respectively. Full and broken lines mark bifurcation points from stable or unstable steady states. The values of the fixed parameters are $\alpha = 3$, $\varepsilon = T^{-1} = 10^{-2}$, and $P = 1$.

appears at

$$\gamma = \sqrt{\frac{(1+2P)}{2\alpha^2}\Delta[\alpha 2\varepsilon P - \alpha\Delta^2 + (1+2P)\varepsilon\Delta]}. \quad (28)$$

The square root is well defined in the intervals $\Delta \leqslant \Delta_-$ and $0 \leqslant \Delta \leqslant \Delta_+$, where

$$\Delta_\pm \equiv \frac{(1+2P)\varepsilon \pm \sqrt{(1+2P)^2\varepsilon^2 + 8\alpha^2\varepsilon P}}{2\alpha} \quad (29)$$

and the graph of $\gamma = \gamma(\Delta)$ leads to the left and right lines denoted by H_2 in Fig. 1. The left branch for $\Delta < 0$ corresponds to the line H_2^- in Fig. 5(b) of Ref. [20] for the case of equal gain coefficients. The critical points $(\Delta,\gamma) = (\Delta_\pm,0)$ and $(\Delta,\gamma) = (0,0)$ are singular points and their unfolding as β increases will be commented in the discussion section. The frequency at the Hopf bifurcation points is given by $\omega = \sqrt{a_3/a_1}$. Inserting the expression of R_1^2 at the Hopf bifurcation, we obtain

$$\omega = \sqrt{2\varepsilon P + (1+2P)\varepsilon\Delta/\alpha}, \quad (30)$$

showing a combination of the relaxation oscillation frequency of the laser and the detuning.

Figure 1 shows the stability domains for the steady states in the injection-versus-detuning parameter space. Figure 1(a) is the diagram when only the TE mode is considered for the slave laser. Figure 1(b) shows the diagram when both the TE and TM modes are considered for the slave laser. Notice that there exists two distinct regions where the mixed-mode steady state is stable (one in the positive and one in the negative detuning range). For higher negative detunings, the lines H_2 and SN_1 intersect, allowing a region of bistability between the TE + TM steady state and the TE steady state [not shown in Fig. 1(b)]. The dot marks a degenerate Hopf bifurcation point (one pair of imaginary eigenvalues and one zero eigenvalue) located at [32]

$$\Delta = \frac{\varepsilon(1+2P)(1+\alpha^2)}{\alpha}. \quad (31)$$

The square marks another degenerate Hopf point (one pair of imaginary eigenvalues and one zero eigenvalue) located at

$$\Delta = \frac{\varepsilon(1+2P)}{\alpha}. \quad (32)$$

Two typical bifurcation diagrams for fixed detuning as a function of injection strength are shown in Fig. 2. It shows the upper and middle branches of the pure-mode R_1^2 in the upper region of the figure and R_1^2 of the mixed-mode emerging from $\gamma = 0$. If Δ is further decreased to large negative detunings, the Hopf bifurcation point H_2 moves to higher intensities allowing the coexistence of stable TE + TM and TE steady states.

C. Case $\beta > 0$

It is interesting to note that the TE pure-mode solution and its stability is independent from the gain ratio k. Although the stability analysis of the TE + TM mixed mode is not as simple as in the previous case, we can obtain the bifurcation boundaries parametrically, see Fig. 3. The region of stability of this mixed-mode solution shrinks when β increases from 0 and finally disappears. The Routh-Hurwitz stability conditions give us an upper bound, β_c, for the presence of a stable mixed-mode solution,

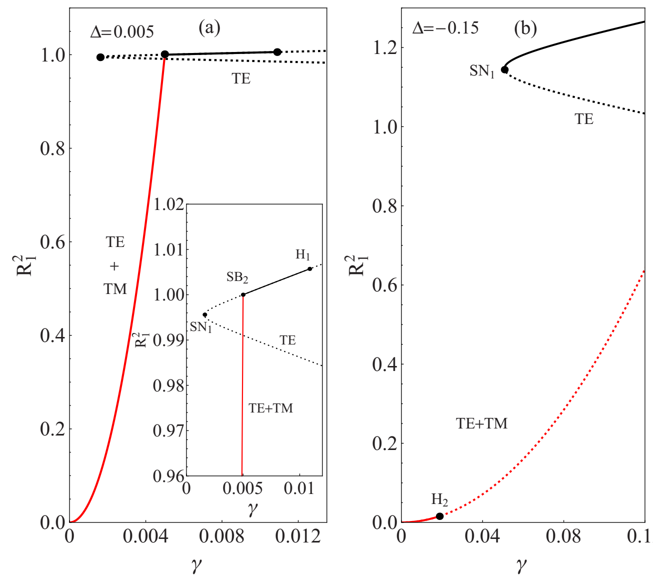

FIG. 2. (Color online) Bifurcation diagram of the steady states as a function of the injection strength γ in the case $\beta = 0$. (a) $\Delta = 0.005$, the mixed mode (TE + TM) exchanges its stability with the pure mode (TE) at SB_2 as illustrated by the closeup. The pure-mode steady state then destabilizes at the Hopf bifurcation point H_1. (b) $\Delta = -0.15$; the mixed-mode destabilizes through a Hopf bifurcation (H_2) while the pure mode stabilizes at SN_1. Other parameters are the same as in Fig. 1.

$$\beta_c = \tfrac{1}{4}[-1 + \sqrt{1 + 4\varepsilon(1+2P)}]. \quad (33)$$

Note the apparition of a new degenerate Hopf bifurcation point (one pair of imaginary eigenvalues and two zero eigenvalues) denoted by a triangle in Fig. 3. Provided that $\beta < \beta_c$, one may activate the unsupported polarization mode by injecting light into the natural supported mode. Figure 4(a) shows a bifurcation diagram in function of the injection strength at $\Delta = 0.035$ where the two steady states exchange their stability at SB_2. Figure 4(b) is a typical bifurcation diagram in the small region of bistability.

III. TM INJECTION

We now investigate the case of orthogonal injection, where light is injected in the unsupported TM mode. In this case, the dimensionless rate equations are given by

$$\frac{dE_1}{dt} = (1+i\alpha)NE_1, \quad (34)$$

$$\frac{dE_2}{dt} = k(1+i\alpha)(N-\beta)E_2 + \gamma\exp(i\Delta t), \quad (35)$$

$$T\frac{dN}{dt} = P - N - (2N+1)(|E_1|^2 + |E_2|^2). \quad (36)$$

The case $k = 1$ ($\beta = 0$) is the same as for the TE injection problem, with the roles of TE and TM being interchanged (see Sec. II B).

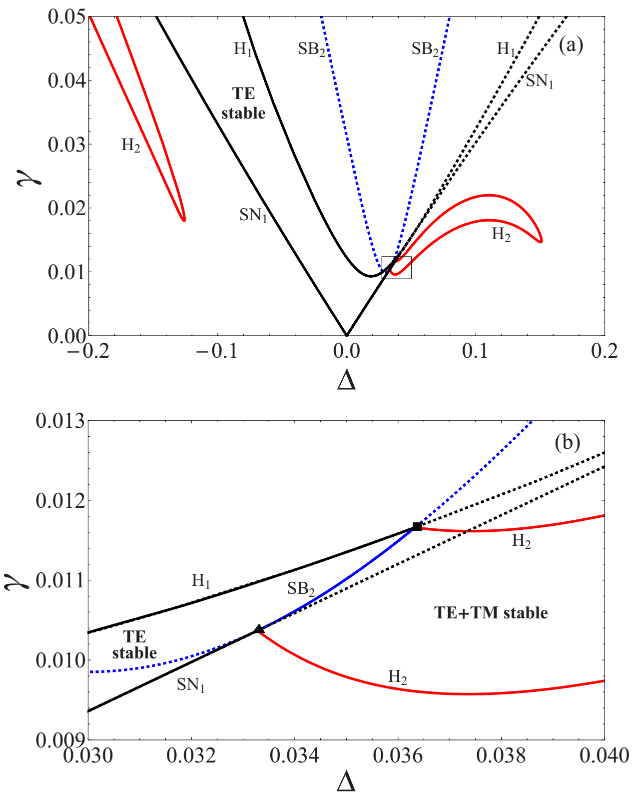

FIG. 3. (Color online) (a) Stability diagram for $\beta = 0.01$ (the values of the other parameters are the same as in Fig. 1). The mixed-mode steady state is stable inside the regions bounded by the Hopf bifurcation H_2. Compared to Fig. 1 for the case $\beta = 0$, the two branches H_2 are now folded and are necking off the $\gamma = 0$ axis. (b) Blow up around the stable part of SB_2. The square marks a degenerate Hopf bifurcation point (one pair of imaginary eigenvalues and one zero eigenvalue). The triangle marks another degenerate Hopf bifurcation point (one pair of imaginary eigenvalues and two zero eigenvalues).

In order to analyze the case $\beta \neq 0$, we introduce $E_2 = R_2 \exp(i\Delta t + i\phi_2)$ and $E_1 = R_1 \exp(i\phi_1)$ into Eqs. (34)–(36) and obtain

$$\frac{dR_1}{dt} = NR_1, \tag{37}$$

$$\frac{dR_2}{dt} = k(N-\beta)R_2 + \gamma\cos(\phi_2), \tag{38}$$

$$\frac{d\phi_2}{dt} = -\Delta + k\alpha(N-\beta) - \gamma R_2^{-1}\sin(\phi_2), \tag{39}$$

$$T\frac{dN}{ds} = P - N - (2N+1)\left(R_1^2 + R_2^2\right), \tag{40}$$

where we have omitted the equation for ϕ_1.

We first compute the steady-state solutions of Eqs. (37)–(40). The pure-mode solution is given by

$$\begin{aligned}(1):\ R_1 &= 0,\\ \gamma^2 &= \{k^2(N-\beta)^2 + [-\Delta + \alpha k(N-\beta)]^2\}R_2^2, \qquad (41)\\ R_2^2 &= \frac{P-N}{1+2N} \geqslant 0.\end{aligned}$$

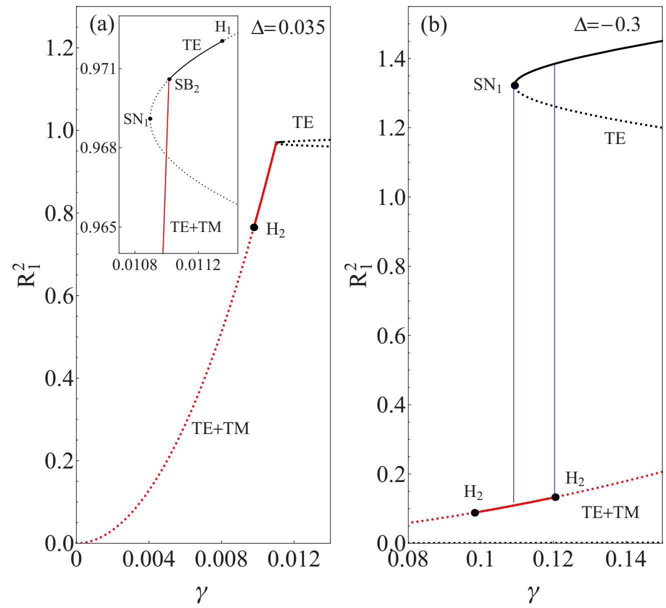

FIG. 4. (Color online) Bifurcation diagram of the steady states as a function of the injection strength γ in the case $\beta = 0.01$. (a) $\Delta = 0.035$; the stability exhange occurs at SB_2, which is very close to SN_1 as illustrated by the closeup. (b) $\Delta = -0.3$; the system exhibits a small region of bistability (delimited by the vertical blue lines) between the pure- and mixed-mode steady states. Other parameters are the same as in Fig. 3.

The mixed-mode solution is

$$\begin{aligned}(2):\ N &= 0,\\ R_1^2 &= P - R_2^2 \geqslant 0, \qquad (42)\\ \gamma &= \sqrt{[k^2\beta^2 + (\Delta + \alpha k\beta)^2]}R_2.\end{aligned}$$

Note that this mixed-mode SS exists only if $R_1^2 \geqslant 0$, which then requires the condition

$$\gamma \leqslant \sqrt{P[k^2\beta^2 + (\Delta + \alpha k\beta)^2]}. \tag{43}$$

In the next section we analyze the stability of these steady states.

A. Stability

1. *TM steady state*

From (37)–(40), we determine the Jacobian matrix and compute the characteristic equation for the growth rate λ. One eigenvalue is

$$\lambda_1 = N. \tag{44}$$

Stability requires $N < 0$. Inserting $N = 0$ into (41), we find a first bifurcation of the pure-mode steady state located at

$$\gamma = \sqrt{[k^2\beta^2 + (\Delta + \alpha k\beta)^2]P}. \tag{45}$$

The three remaining eigenvalues satisfy

$$\lambda^3 + a_1\lambda^2 + a_2\lambda + a_3 = 0, \tag{46}$$

where

$$a_1 = -2k(N-\beta) + \varepsilon\frac{1+2P}{1+2N},$$
$$a_2 = \{k^2(N-\beta)^2 + [\Delta - k(N-\beta)\alpha]^2\} - 2\varepsilon k\frac{1+2P}{1+2N}(N-\beta) + \varepsilon 2k(P-N),$$
$$a_3 = \varepsilon\frac{1+2P}{1+2N}\{k^2(N-\beta)^2 + [-\Delta + k(N-\beta)\alpha]^2\} + 2\varepsilon k(P-N)[\Delta\alpha - k(N-\beta)(\alpha^2+1)]. \quad (47)$$

Introducing

$$X = \Delta - k(N-\beta)\alpha, \quad (48)$$

the saddle-node or limit point condition is $a_3 = 0$ or, equivalently,

$$0 = \frac{1+2P}{1+2N}[k^2(N-\beta)^2 + X^2] + 2k(P-N)[\alpha X - k(N-\beta)]. \quad (49)$$

The Hopf bifurcation condition is $a_1a_2 - a_3 = 0$ or, equivalently,

$$0 = (N-\beta)X^2 + \varepsilon(P-N)\alpha X + k^2(N-\beta)^3 - \varepsilon\frac{1+2P}{1+2N}[2k(N-\beta)^2 + \varepsilon(P-N)] + \varepsilon k(P-N)(N-\beta) - \varepsilon^2\left(\frac{1+2P}{1+2N}\right)^2(N-\beta). \quad (50)$$

These two conditions lead to the neutral lines SN_1 and H_1.

2. TE+TM steady state

The characteristic equation for the growth rate λ of the mixed-mode solution is

$$\lambda^4 + a_1\lambda^3 + a_2\lambda^2 + a_3\lambda + a_4 = 0, \quad (51)$$

where

$$a_1 = 2k\beta + \varepsilon(1+2P),$$
$$a_2 = \left[k^2\beta^2 + (\Delta + k\alpha\beta)^2 + \varepsilon(1+2P)2k\beta + 2\varepsilon k R_2^2 + 2\varepsilon R_1^2\right],$$
$$a_3 = \varepsilon\left\{(1+2P)(k^2\beta^2 + (\Delta + k\alpha\beta)^2) + 2kR_2^2[(\Delta + k\alpha\beta)\alpha + k\beta]4R_1^2k\beta\right\},$$
$$a_4 = 2\varepsilon R_1^2[k^2\beta^2 + (\Delta + k\alpha\beta)^2]. \quad (52)$$

The Routh-Hurwitz conditions for the stability of the steady state are given by (20). The Hopf condition $a_1a_2a_3 - a_3^2 - a_1^2a_4 = 0$ is solved for R_1^2. We then use (42) to determine the Hopf bifurcation line H_2 in the (Δ,γ) parameters plane.

Figure 5 shows a stability diagram for injection in the unsupported TM mode of the diode laser. The Hopf bifurcation H_1 of the pure-mode solution is everywhere unstable and is not drawn for clarity. The triangle marks a degenerate bifurcation point (one pair of imaginary eigenvalues and two zero eigenvalues) located at

$$\Delta_c = \frac{k\sqrt{\alpha^2P^2 - \beta^2(2P+1)^2 - 2\beta P(2P+1)} - \alpha kP}{2P+1} - \alpha\beta k. \quad (53)$$

Note that there is only one H_2 branch. The two branches H_2 in Fig. 1 for the case $\beta = 0$ disappear as soon as β slightly increases leading place to the one shown in Fig. 5 for moderately small values of β. For $\Delta > \Delta_c$ both the mixed mode and the pure mode are stable and are connected at the SB_2 line. The saddle-node bifurcation line SN_1 is unstable (dashed

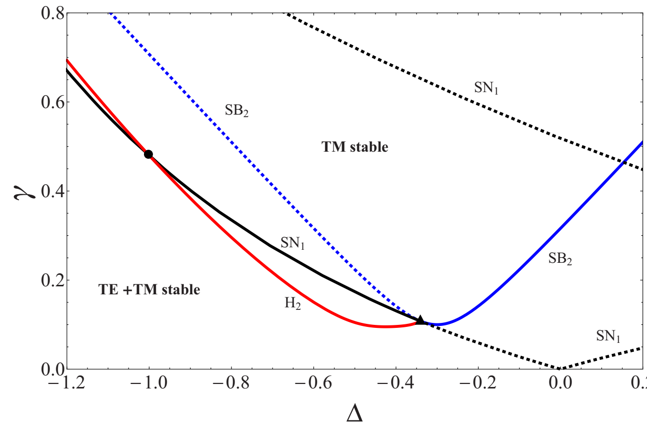

FIG. 5. (Color online) Stability diagram of the orthogonal injection case for $\beta = 0.125$ ($k = 0.8$). The other parameters and the notation for the bifurcations are the same as in Fig. 1.

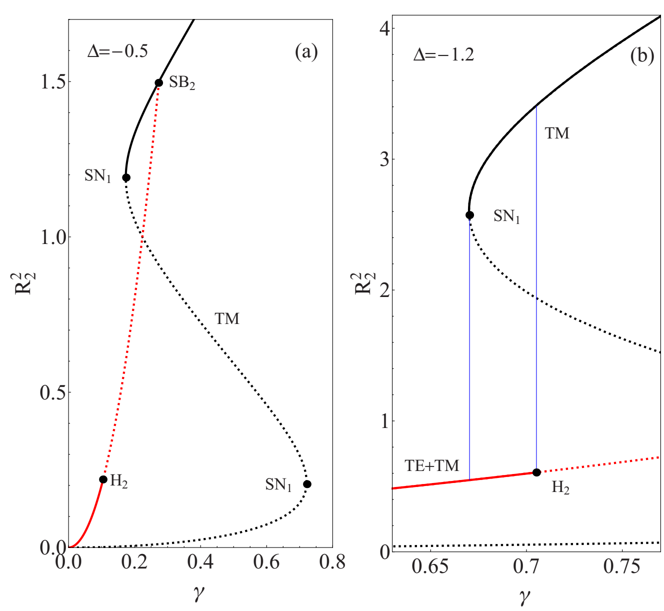

FIG. 6. (Color online) Bifurcation diagram of the steady states as a function of the injection strength γ. (a) $\Delta = -0.5$, the mixed mode destabilizes through a Hopf bifurcation while the pure mode stabilizes through SN_1. (b) $\Delta = -1.2$, the system exhibits a small region of bistability (delimited by the vertical blue lines) between the pure- and mixed-mode steady states. Other parameters are the same as in Fig. 5.

line), and the pure mode remains unstable to the SB_2 line. For $\Delta < \Delta_c$ the mixed mode undergoes a Hopf bifurcation before the stable pure mode emerges at the SN_1 stable line. The bifurcation diagram of Fig. 6(a) illustrates this case. The dot in Fig. 5 marks another degenerate bifurcation point (one pair of imaginary eigenvalues and one zero eigenvalue). For larger negative detunings, a region of bistability between mixed-mode and single-mode steady states is possible, as shown in Fig. 6(b). It is this particular domain that was explored in detail in Ref. [20].

IV. DISCUSSION

In this paper, we analyzed the steady states and their linear stability properties for a two polarization mode laser subject to either TE or TM injection. Representative bifurcation diagrams highlight particular features of the stability diagrams. We did not explore the onset of higher-order instabilities or four-wave mixing regimes which appear outside the locking regions.

The problem with TE injection into the dominant TE mode is well documented in the literature. But, to our knowledge, the problem has never been explored analytically when both TE and TM modes are taken into account for the slave laser. We show that, provided the gain coefficients do not differ too much, there is the possibility of finding stable mixed-mode steady states. In terms of our parameter β which is proportional to the small difference between the gain coefficients, we provide an upper bound β_c below which they can appear. Using (33) and taking advantage of the fact that $\varepsilon = 10^{-2} << 1$, β_c admits the asymptotic approximation

$$\beta_c = \frac{\varepsilon}{2}(1 + 2P), \tag{54}$$

where we recognize the expression of the relaxation oscillation damping rate of the solitary laser. If $\beta > \beta_c$, we recover the previously known stability diagram for the locking of a single -mode steady state. If $\beta < \beta_c$ and the detuning is sufficiently negative, the coexistence of stable mixed-mode and single-mode steady states is possible. Taking a typical photon lifetime of 9.0×10^{-11} s, a detuning of 1 GHz corresponds to $\Delta = 0.09$. The region of bistability appears at a detuning of a few ($\sim$−4) GHz, which is realizable experimentally [33]. This does not mean that the coexistence between two single-mode steady states is excluded. Earlier studies of optical bistability considered injected SLs operating close to the laser threshold [34]. More recently, bistability between TE modes was observed for an injected quantum-dot SL [35].

In the case of a two-mode laser subject to TM injection, the stability diagrams have been explored in detail both experimentally and numerically in Refs. [20,33]. The onset of higher-order instabilities to tori and chaos has also been examined in Ref. [33]. Here we show that a fully analytical approach is possible if we ignore gain saturation but consider different constant gains.

For both the classical TE injection or orthogonal TM injection problems, we have stressed the importance of considering the case of equal gain coefficients as the starting point of all studies. This reduced problem is valid for both cases and its stability diagram can be used to properly formulate our questions. We discuss two issues related to the bistability between pure and mixed-mode steady states. We first determine the bistability conditions by finding when the curve H_2 intersects the line SN_1 for $\Delta < 0$ (Fig. 1). Assuming $\Delta = O(\varepsilon^{1/2})$, we find from (28)

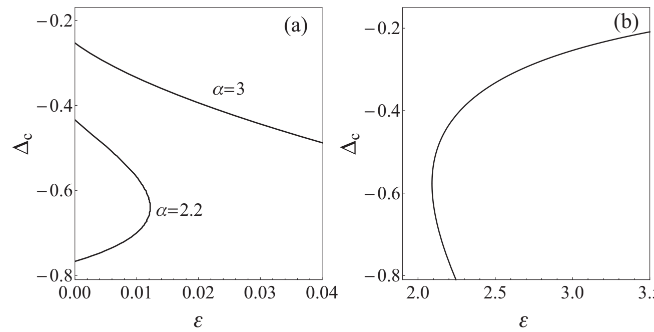

FIG. 7. Critical detuning satisfying the condition $\gamma_{H_2} = \gamma_{SN_1}$. $P = 1$. (a) $\Delta_c = \Delta_c(\varepsilon)$ is represented for $\alpha = 2.2$ and $\alpha = 3$. (b) $\Delta_c = \Delta_c(0)$ is represented as a function of α. If $\alpha < \alpha_c \simeq 2.1$, then there are no solutions.

$$\gamma_{H_2} \simeq \sqrt{\frac{1 + 2P}{2\alpha^2}\Delta(2\alpha\varepsilon P - \alpha\Delta^2)}, \tag{55}$$

where $\Delta < -\sqrt{2\varepsilon P}$. The line SN_1 does not depend on ε. Assuming that $|\Delta|$ and $|N| = O(|\Delta|)$ are small, we obtain from (10) and (16)

$$\gamma_{SN_1} \simeq \frac{\Delta}{\sqrt{1+\alpha^2}}\sqrt{\frac{P(1+\alpha^2) - \alpha\Delta}{1 + \alpha^2 + 2\alpha\Delta}}. \tag{56}$$

The critical point $\Delta = \Delta_c(\varepsilon) < 0$ for the intersection of $\gamma_{H_2}(\Delta)$ and $\gamma_{SN_1}(\Delta)$ then leads to the implicit solution

$$\varepsilon = \frac{1}{2P}\left[\Delta_c^2 + \frac{2\alpha\Delta_c(P(1+\alpha^2) - \alpha\Delta_c)}{(1+2P)(1+\alpha^2)(1+\alpha^2+2\alpha\Delta_c)}\right]. \tag{57}$$

The solution is shown in Fig. 7(a) for two different values of α. There is a critical value of $\alpha = \alpha_c \simeq 2.1$ below which there are no intersections of $\gamma_{H_2}(\Delta)$ and $\gamma_{SN_1}(\Delta)$. Slightly above α_c, there are two intersections in the negative detuning range, see Fig. 7(b). We also can deduce from (57) that $|\Delta_c|$ increases monotonically with P. Consequently, the bistability phenomenon could be captured for lower values of the detuning by decreasing P. For the values of the fixed parameters used in this paper, we find the first intersection at $\Delta_c = -0.33$ which is a good approximation of the critical point. For higher negative Δ_c, the approximation (57) becomes progressively less accurate. Second, we note that the coexistence between a pulsating TE+TM time-periodic regime and a single TE steady state is also possible [see Figs. 4(b) and 6(b)]. The frequency of the oscillations is provided by (30), in the first approximation. Its dominant contribution comes from the relaxation oscillation frequency of the solitary laser if $|\Delta| = O(\varepsilon^{1/2})$.

Last, we discuss the case of the singular points $(\Delta_\pm, 0)$. The H_2 curve dramatically unfolds near these points if the gain coefficients begin to differ. In the case of small gain saturation, it was shown that H_2 unfolds into two branches, H_2^- and H_2^+ (Fig. 5 of Ref. [20]). If we introduce a small β, then we have found a similar phenomenon in our case.

ACKNOWLEDGMENTS

G.F. acknowledges the support of the Belgian F.R.I.A. T.E. acknowledges the support of the F.N.R.S. (Belgium) and fruitful discussions with A. Amann in 2009. This work benefitted from the support of the Interuniversity Attraction Poles program of the Belgian Science Policy Office under Grant No. IAP P7-35 "photonics@be."

[1] N. Patel, J. Ripper, and P. Brosson, IEEE J. Quantum Electron. **9**, 338 (1973).
[2] Y. C. Chen and J. M. Liu, Appl. Phys. Lett. **45**, 731 (1984).
[3] N. K. Dutta, J. Appl. Phys. **55**, 285 (1984).
[4] Y. C. Chen and J. M. Liu, Appl. Phys. Lett. **46**, 16 (1985).
[5] Y. C. Chen and J. M. Liu, Appl. Phys. Lett. **50**, 1406 (1987).
[6] A. Sapia, P. Spano, and B. Daino, Appl. Phys. Lett. **50**, 57 (1987).
[7] Y. Mori, J. Shibata, and T. Kajiwara, Appl. Phys. Lett. **51**, 1971 (1987).
[8] Y. Mori, J. Shibati, and T. Kajiwara, IEEE J. Quantum Electron. **25**, 265 (1989).
[9] Y. Mori, J. Shibata, and T. Kajiwara, J. Appl. Phys. **67**, 2223 (1990).
[10] F. Mogensen, H. Olesen, and G. Jacobsen, Electron. Lett. **21**, 696 (1985).
[11] O. Lidoyne, P. Gallion, and D. Erasme, IEEE J. Quantum Electron. **27**, 344 (1991).
[12] K. Kikuchi, C.-E. Zah, and T.-P. Lee, J. Lightw. Technol. **6**, 1821 (1988).
[13] L. Goldberg, H. Taylor, J. Weller, and D. Bloom, Electron. Lett. **19**, 491 (1983).
[14] R. Hui, A. Mecozzi, A. D'Ottavi, and P. Spano, Electron. Lett. **26**, 997 (1990).
[15] G. Liu, X. Jin, and S. L. Chuang, IEEE Photon. Technol. Lett. **13**, 430 (2001).
[16] G. H. M. van Tartwijk and D. Lenstra, Quantum Semiclass. Opt. **7**, 87 (1995).
[17] S. Wieczorek, B. Krauskopf, T. Simpson, and D. Lenstra, Phys. Rep. **416**, 1 (2005).
[18] S. Wieczorek, T. B. Simpson, B. Krauskopf, and D. Lenstra, Phys. Rev. E **65**, 045207 (2002).
[19] T. Erneux and P. Glorieux, *Laser Dynamics* (Cambridge University Press, Cambridge, UK, 2010).
[20] S. Osborne, K. Buckley, A. Amann, and S. O'Brien, Opt. Express **17**, 6293 (2009).
[21] I. Gatare, M. Sciamanna, M. Nizette, and K. Panajotov, Phys. Rev. A **76**, 031803 (2007).
[22] M. Sorel, P. J. R. Laybourn, A. Scirè, S. Balle, G. Giuliani, R. Miglierina, and S. Donati, Opt. Lett. **27**, 1992 (2002).
[23] W. Coomans, S. Beri, G. VanderSande, L. Gelens, and J. Danckaert, Phys. Rev. A **81**, 033802 (2010).
[24] G. Smolyakov and M. Osinski, IEEE J. Quantum Electron. **47**, 1463 (2011).
[25] T. Heil, A. Uchida, P. Davis, and T. Aida, Phys. Rev. A **68**, 033811 (2003).
[26] Y. Takeuchi, R. Shogenji, and J. Ohtsubo, Appl. Phys. Lett. **93**, 181105 (2008).
[27] Y. Takeuchi, R. Shogenji, and J. Ohtsubo, Opt. Rev. **17**, 144 (2010).
[28] K. Hicke, M. Escalona-Moran, D. Brunner, M. Soriano, I. Fischer, and C. Mirasso, IEEE J. Sel. Top. Quantum Electron. **19**, 1501610 (2013).
[29] G. Friart, G. Verschaffelt, J. Danckaert, and T. Erneux, Opt. Lett. **39**, 6098 (2014).
[30] G. Friart, L. Weicker, J. Danckaert, and T. Erneux, Opt. Express **22**, 6905 (2014).
[31] J. Uspensky, *Theory of Equations* (McGraw-Hill, New York, 1948).
[32] A. Gavrielides, V. Kovanis, and T. Erneux, Opt. Commun. **136**, 253 (1997).
[33] D. O'Shea, S. Osborne, N. Blackbeard, D. Goulding, B. Kelleher, and A. Amann, Opt. Express **22**, 21701 (2014).
[34] T. Erneux, A. Gavrielides, and V. Kovanis, Quantum Semiclass. Opt. **9**, 811 (1997).
[35] T. Erneux, E. A. Viktorov, B. Kelleher, D. Goulding, S. P. Hegarty, and G. Huyet, Opt. Lett. **35**, 937 (2010).